Determination of ionic polarizability by nonsequential double ionization

MingZheng Wei,[1] HuiPeng Kang,[2,3,*] YanLan Wang,[2,3] Wei Quan,[2,3] Jing Chen,[4,5,†] ChuanXi Duan,[1] and XiaoJun Liu[2,3,‡]

[1]*College of Physical Science and Technology, Central China Normal University, Wuhan 430079, China*
[2]*State Key Laboratory of Magnetic Resonance and Atomic and Molecular Physics, Wuhan Institute of Physics and Mathematics, Innovation Academy for Precision Measurement Science and Technology, Chinese Academy of Sciences, Wuhan 430071, China*
[3]*University of Chinese Academy of Sciences, Beijing 100049, China*
[4]*Hefei National Research Center for Physical Sciences at the Microscale and School of Physical Sciences, Department of Modern Physics, University of Science and Technology of China, Hefei, China*
[5]*Shenzhen Key Laboratory of Ultraintense Laser and Advanced Material Technology, and College of Engineering Physics, Shenzhen Technology University, Shenzhen 518118, China*

(Received 15 February 2023; accepted 18 July 2023; published 8 August 2023)

We report on a theoretical study of nonsequential double ionization (NSDI) of magnesium atoms by circularly polarized intense laser pulses. We introduce a concise model considering the laser-induced dynamic core polarization, which is an often overlooked effect in understanding strong-field double ionization. By tracing back the electron trajectories, we demonstrate how the ionic response to the instantaneous laser field enhances the NSDI probability, which plays a crucial role in circular polarization. Furthermore, we propose a method to extract the ionic polarizability from the ratio of double to single ionization. This scheme can be applied to other polar targets and serves as a potential way to probe nonequilibrium states of strongly driven systems on the subfemtosecond timescale.

DOI: 10.1103/PhysRevA.108.023111

I. INTRODUCTION

Electron correlation plays an important role in many fundamental processes in light-driven atomic and molecular systems. The development in ultrafast laser technology has provided a valuable means to study and control electron correlation with unprecedented spatial and temporal resolution. One intriguing example is the correlated emission of two electrons from atoms and molecules irradiated by femtosecond intense laser fields, coined as nonsequential double ionization (NSDI). Since its discovery, NSDI has attracted tremendous attention [1,2]. This phenomenon shows a characteristic knee structure, known as a dramatic enhancement in the double ion yield versus intensity curve, which is much larger than the prediction of the sequential tunneling theory [3]. Nowadays, it is commonly accepted that the mechanism of NSDI can be understood within the quasiclassical recollision model [4]. In this model, first the outmost electron tunnels through the distorted Coulomb potential barrier suppressed by the intense laser field; then, the freed electron is accelerated by the oscillating laser field; finally, when the laser field changes its sign, the electron may return to the parent ion core, where it can ionize another electron via inelastic scattering. This physical picture has also been successfully applied to many other strong-field ionization phenomena such as high-order-harmonic generation [5] and above-threshold ionization [6].

According to the recollision picture, NSDI probability will be significantly suppressed in circularly polarized (CP) fields. This is because a transverse drift velocity, resulting from the additional transverse electric field component of the laser light, can make the freed electron spiral away from the core, which suppresses the recollision and thus NSDI yield. Earlier experiments on strong-field double ionization of the noble gas atoms have confirmed this view. For example, the knee structure disappears when using CP laser pulses for He [7] and Ar [8]. However, later experiments on NO, O_2 molecules [8], and Mg atoms [9] discovered unexpected knee structure in the ion yield curve for double ionization with CP light.

As a nearly ideal two-electron system with various doubly excited states exhibiting a high degree of electron correlation, Mg has been widely used to study the interesting feature of NSDI. Recently, a number of classical or semiclassical simulations revealed that recollision is still responsible for the surprising knee structure, i.e., NSDI with circular polarization for Mg [10–13]. It was shown that the recollision probability crucially depends on the initial transverse velocity of the tunneled electron and the atomic species [12]. Experimentally, it has been identified that the NSDI of Mg mainly occurs via the ionic excited state $Mg^{+*}(3p\ ^2P_{3/2,1/2})$ pumped by the returning electron, while the direct ionization channel induced by recollision plays a negligible role [14].

Although the previous works have been continuously advancing our understanding of NSDI [10–13], there is seldom study focused on the influence of the remaining electrons' motion on NSDI right after tunneling of the first electron. Since such motion is closely related to the dipole potential in the laser fields, it can be used to examine the multielectron

*kanghp@wipm.ac.cn
†chenjing@ustc.edu.cn
‡xjliu@wipm.ac.cn

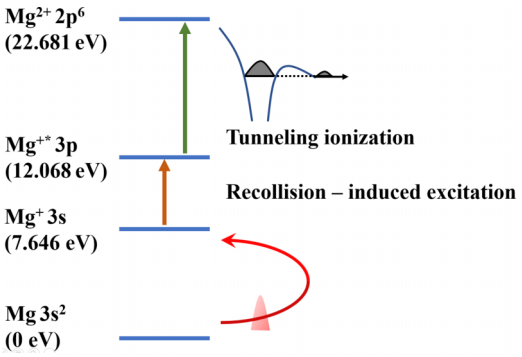

FIG. 1. The diagram of a recollision-induced ESI channel leading to Mg^{2+}.

effects. Because Mg^+ has a large static polarizability and the remaining electrons can be easily influenced by the laser light, Mg has been regarded as an appropriate system aiming at studying the role of the ionic core polarization in strong-field ionization. Shvetsov-Shilovski *et al*. investigated the role of the laser-induced dipole potential in the formation of the photoelectron momentum distributions with a wide range of laser intensities and wavelengths in elliptically polarized fields [15]. In Ref. [16], it has been shown that the ionic core polarization affects the recolliding electrons during the photoionization process and clearly enhances the relative yields of the low-energy structure and very low-energy structure. It is well known that NSDI is closely related to the energy and momentum distributions of the returning electrons [14]. However, whether and how the laser-induced dipole potential influences NSDI is unclear.

In this paper, we present a detailed investigation of the effects of the laser-induced dipole potential on the NSDI of Mg by CP light. We perform a three-dimensional (3D) Monte Carlo model simulation including the dynamic dipole potential. Our analysis of the electron trajectories reveals that the dipole potential focuses the recolliding electrons and thus enhances the double ionization yields. Additionally, we propose a method allowing us to extract the static polarizability of the Mg^+ ion from the ratios of Mg^{2+}/Mg^+.

This paper is organized as follows. The theoretical model is presented in Sec. II. In Sec. III, we display and discuss the results, and the conclusions are shown in Sec. IV.

II. THEORETICAL MODEL

In the spirit of the recollision picture, the returning electron can induce an impact direct ionization, i.e., $(e, 2e)$ process or an excitation with subsequent ionization (ESI) [17–20]. For the latter, the excited electrons are assumed to be subsequently ionized by the remaining laser field [21,22], as shown in Fig. 1. It has been shown that the ionic excited state $Mg^{+*}(3p\ ^2P_{3/2,1/2})$ induced by recollision mainly contributes to the NSDI of Mg, while the $(e, 2e)$ pathway plays a minor role [14]. Following that finding, in this paper we mainly consider the contribution of the ESI channel via the $Mg^{+*}(3p\ ^2P_{3/2,1/2})$ state. In our model, the NSDI ratio is proportional to the effective energy-averaged cross section, which can be expressed as

$$R = \frac{\int dE_{\rm ret}\sigma(E_{\rm ret})W_{\rm ret}(E_{\rm ret})P_{\rm exc}}{\int dE_{\rm si}W_d(E_{\rm si})}, \tag{1}$$

where $E_{\rm ret}$ and $E_{\rm si}$ are the energy of the returning electron and of the directly ionized electron that accounts for the single ionization event, for the numerator and denominator, respectively; $\sigma(E_{\rm ret})$ is the field-free impact excitation cross section obtained from the previous experiments on Mg [23,24], $W_{\rm ret}(E_{\rm ret})$ is the returning energy distribution, $P_{\rm exc}$ is the instantaneous Ammosov-Delone-Krainov (ADK) ionization probability of the ionic excited state, and $W_d(E_{\rm si})$ denotes the energy distribution of the directly ionized electrons that account for the single ionization events. Here we consider that the ionization of the second electron mainly occurs within the half cycle after recollision. In this model, the ionization probability of the ionic excited state is given by

$$P_{\rm exc} = I_{\rm pexe}C^2_{n^*l}\frac{(2l+1)(l+|m|)!}{2^{|m|}(|m|)!(l-|m|)!}\left(\frac{2(2I_{\rm pexe})^{\frac{3}{2}}}{|F|}\right)^{2n^*-1}$$
$$\times * \exp[-2(2I_{\rm pexe})^{\frac{3}{2}}/3|F|], \tag{2}$$

where $I_{\rm pexe}$ represents the ionization potential of the ionic excited state, $C^2_{n^*l}$ can be calculated by $(\frac{2e}{n^*})^{n^*}\frac{1}{\sqrt{2\pi n^*}}$ with the e constant and the effective principal quantum number. $n^* = 1/\sqrt{2I_{\rm pexe}}$, and l and m are the orbital angular momentum and the magnetic quantum numbers, respectively.

Next, we resort to a 3D Monte Carlo model simulation to obtain $W_{\rm ret}(E_{\rm ret})$ and $W_d(E_{\rm si})$. The electron trajectories at each time step during the laser pulse are determined by the classical Newtonian equation of motion,

$$\frac{d^2\mathbf{r}}{dt^2} = -\mathbf{F}(t) - \nabla V(\mathbf{r}, t). \tag{3}$$

Here we consider the following CP electric field in the (x, z) plane:

$$\mathbf{F}(t) = a(t)F_0[\sin(\omega t)\mathbf{e_x} + \cos(\omega t)\mathbf{e_z}], \tag{4}$$

with the amplitude F_0 and the laser frequency ω. The envelope function $a(t)$ is a constant equal to 1 for the first 11 cycles (700 nm) or 10 cycles (800 nm) and is reduced to 0 with a three-cycle ramp in the form of $\cos^2$, corresponding to a pulse duration of 30 fs for both wavelengths. When including the polarization effect, the ionic potential has the following form:

$$V(\mathbf{r}, t) = -1/r - \alpha_I\mathbf{F(t)}\cdot\mathbf{r}/r^3, \tag{5}$$

where α_I is the static polarizability of the singly charged ion. The second term denotes the induced dipole potential. For $r \to 0$, we set a cutoff at a point where the laser field can be counteracted by the core polarization [14,25]. The cutoff point r_c is solved by $\alpha_I F(t)/r_c^2 - r_c F(t) = 0$, which reduces to $r_c = \alpha_I^{1/3}$. As $r \leqslant r_c$, the polarization effects will no longer have an influence on the electron because of the shielding of the ionic system. Therefore, it is necessary to take into account this cutoff point in the calculation.

Based on the tunneling ionization theory [26], one can obtain the initial conditions including the initial position and velocity of the electron trajectory to solve Eq. (3). With a similar method as used in Refs. [27,28], in our calculation

for a CP field, we first calculate the initial conditions in the rotated coordinate and then project them to the original coordinate. At each tunneling instant t_0, the z axis is rotated to be along the instantaneous electric field direction. For the initial position in the rotated coordinate, the coordinates are $x'_0 = y'_0 = 0$ and $z'_0 = -I_p/F(t_0)$ [29,30], where $I_p = I_p(0) + 1/2(\alpha_N - \alpha_I)F_0^2$ denotes the Stark-shifted ionization potential, with $I_p(0)$ the field-free ionization potential and α_N the static polarizability of the atom. Correspondingly, in the original coordinate, the initial positions of the tunnel ionized electron are $x_0 = I_p/F(t_0)\sin\{\arctan[\tan(\omega t_0)]\}$, $y_0 = 0$, and $z_0 = I_p/F(t_0)\cos\{\arctan[\tan(\omega t_0)]\}$. In addition, for the initial velocity in the rotated coordinate, the tunneled electron has a zero longitudinal velocity and a nonzero velocity $\upsilon_\perp$ having a Gaussian distribution in the perpendicular direction of the laser polarization z' axis. Correspondingly, the initial velocities in the rotated coordinate are $v'_{x0} = \upsilon_\perp\cos\theta$, $v'_{y0} = \upsilon_\perp\sin\theta$, and $v'_{z0} = 0$, where θ is the angle between $\upsilon_\perp$ and the transverse direction of the polarization plane, i.e., the x' axis. Thus, in the original coordinate, the corresponding velocities of the electron are $v_{x0} = \upsilon_\perp\cos\theta\cos\{\arctan[\tan(\omega t_0)]\}$, $v_{y0} = \upsilon_\perp\sin\theta$, and $v_{z0} = -\upsilon_\perp\cos\theta\sin\{\arctan[\tan(\omega t_0)]\}$. For each tunneling trajectory, the rate is given by the ADK formula [26,31,32].

For a particular intensity I, an ensemble of 10^6 trajectories is randomly distributed in the time interval $-\pi/2 \leqslant \omega t \leqslant \pi/2$ for a Mg atom, $I_p(0) = 0.2811$ a.u. (7.646 eV). To get $W_{\rm ret}(E_{\rm ret})$, we collect the recollision trajectories and calculate the impact energies. Here, we define the recollision as an event in which the distance between the electron and the core is less than the tunneling exit point after 0.7 T from the tunneling instant [33]. $W_d(E_{\rm si})$ can be obtained by picking the directly ionized electron trajectories. Finally, by summing up these trajectories, the NSDI ratio can be obtained according to Eq. (1).

In the model calculations, the static polarizabilities of the Mg atom and the Mg^+ ion are 71.33 and 35.00 a.u. [15], respectively. The cutoff point r_c is determined to be 3.27 a.u.

III. RESULTS AND DISCUSSION

As shown in Fig. 2(a), the simulation with inclusion of the dipole potential at 800 nm is in good agreement with the experimental data from Ref. [9]. For intensities above $\sim 3 \times 10^{13}$ W/cm^2, the calculations are smaller than the experimental data. This is because sequential double ionization dominates at such intensities, which is beyond the applicable range of our model. To make a more direct comparison between the theoretical calculations and experiments, the laser pulse width for the simulation is 120 fs, which is the same as used in Ref. [9]. In Fig. 2(b), our model simulation also reproduces the ellipticity dependence of the ratio of Mg^{2+}/Mg^+ at 1.5×10^{13} W/cm^2, which coincides with the conclusion of Ref. [9] that the ratio becomes higher as the ellipticity is closer to 0. For the intensities studied here, the Keldysh parameter ranges from about 1.5 to 2.1, indicating that we are working in the transition region between the tunneling ionization and multiphoton ionization mechanisms. In this region, the ADK simulation is found to be in good agreement with the experimental ionization probability of Mg [34].

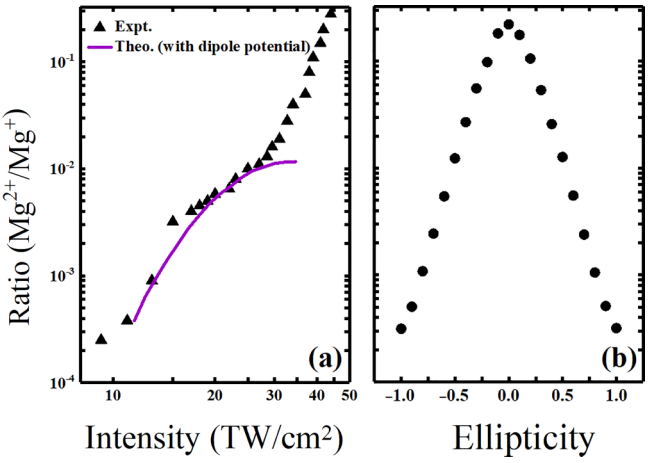

FIG. 2. (a) The ratio of Mg^{2+}/Mg^+ vs laser intensity for 120 fs, 800 nm pulses. Experimental data are from Ref. [9]. The intensity has been divided by 1.3 for the simulation, considering the experimental uncertainty of the intensity calibration. (b) Ellipticity dependence of the ratios of Mg^{2+}/Mg^+ at 1.5×10^{13} W/cm^2.

Figure 3 shows the ratios of Mg^{2+}/Mg^+ as functions of laser intensity with and without the dipole potential included. We also calculate the NSDI ratios of 700 nm for comparison, which are significantly larger than the ones for 800 nm. Furthermore, for each wavelength, one can find that the simulation without inclusion of the dipole potential becomes smaller and smaller than that considering the dipole potential with increasing intensity. This indicates that the dipole potential plays a key role in the NSDI of Mg in CP fields. For higher intensities, the calculation decreases with increasing intensity for each wavelength. This is because the electron can be steered away from the core more easily at high intensities, prohibiting the recollision and NSDI.

To explain the much higher NSDI probability at 700 nm, we compare the initial transverse velocity υ_x (along the x axis here) and corresponding returning energy distributions of the recollision events for both wavelengths at 3×10^{13} W/cm^2,

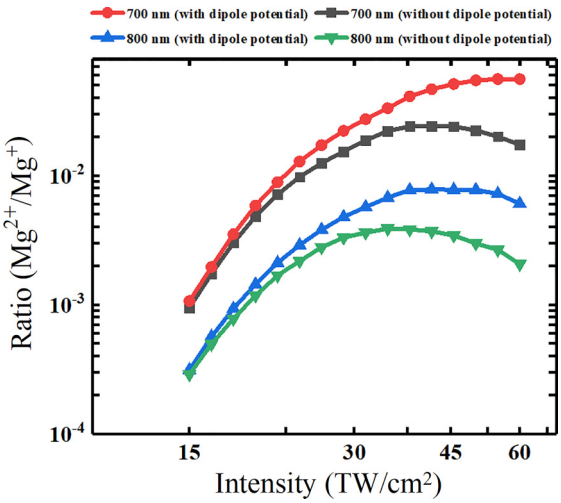

FIG. 3. The ratio of Mg^{2+}/Mg^+ vs laser intensity for 700 and 800 nm. The pulse width is 30 fs for both wavelengths.

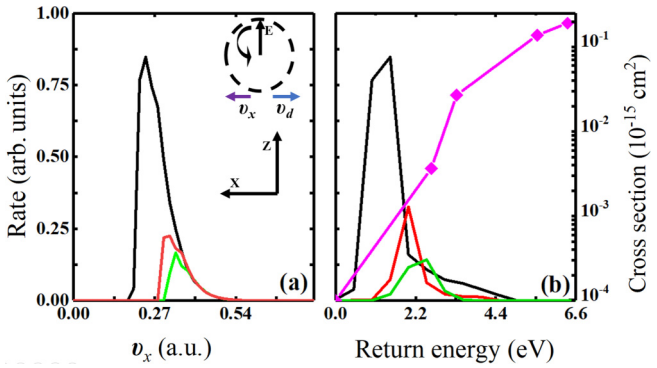

FIG. 4. (a) The initial transverse velocity and (b) corresponding returning energy distributions of the recollision trajectories leading to NSDI, for 700 nm (black lines) with the dipole potential included and 800 nm with (red lines) and without (green lines) the dipole potential included at 3×10^{13} W/cm^2. Without loss of generality, here we consider that the electron tunnels through the distorted Coulomb potential barrier when the instantaneous field direction is along the x axis, with a drift velocity υ_d along the x axis, as shown in the inset of (a). The excitation cross sections used in our model simulations are shown in (b) for reference. The diamonds are the experimental data extracted from [23,24] and the line connects the diamonds.

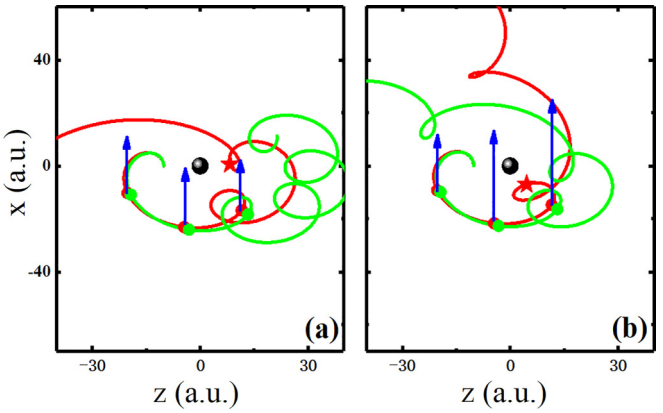

FIG. 5. Characteristic electron trajectories in the laser polarization plane at 3×10^{13} W/cm^2 for 800 nm. Here the electron tunneling occurs when the laser field is along the z axis, as depicted in the inset of Fig. 4(a). (a) The red line shows the recollision trajectory with the initial transverse momentum $\upsilon_x = 0.36$ a.u. when the dipole potential is included. For comparison purpose, we present the green line showing the trajectory with the same initial conditions, but ignoring the dipole potential. (b) Same as (a), but for $\upsilon_x = 0.38$ a.u. The black globe indicates the core and the dots mark the instants around 0.5, 0.75, and 1.0 T after tunneling for every trajectory. The stars mark the instants when the electron is closest to the core for the recollision trajectories. The arrows represent the induced dipole forces, with the scale and direction showing the magnitude (relatively) and direction of the force at different times along the x axis, respectively.

as shown in Fig. 4. The main peak of the υ_x distribution for 700 nm shifts towards the smaller momentum region, with considerably higher rate than the result for 800 nm. This behavior can be understood as follows. In CP fields, the electron tunneling through the distorted Coulomb potential barrier obtains a drift velocity $\upsilon_d = -F_0/\omega$. Neglecting the possible tunneling delay time, such velocity is perpendicular to the instantaneous field direction and steers the electron away from the core. In order to trigger efficient recollision, the electron requires an appropriate initial transverse velocity to compensate for the drift velocity, as depicted in the inset of Fig. 4(a). For 700 nm, the required υ_x is smaller, as the drift velocity is smaller, leading to a much higher tunneling rate due to its exponential scale with the initial transverse velocity [26]. In our model, the NSDI of Mg occurs mainly via recollision-induced ESI. Therefore, the NSDI probability is closely related to the returning energy distribution which depends on the wavelength sensitively [14]. In Fig. 4(b), although the corresponding excitation cross sections are around two times smaller for 700 nm, the weight of the returning electron distribution is much higher, resulting in larger NSDI yields as compared with the 800 nm case.

In order to understand how the dipole potential enhances the NSDI probability, we compare the υ_x distributions with and without the dipole potential included for 800 nm, shown in Fig. 4. The calculations at 700 nm show similar behaviors. When the dipole potential is considered, the required υ_x becomes smaller [Fig. 4(a)] due to the influence of the dipole potential on the recolliding trajectories, as we will discuss later; in addition, the returning energy distribution shifts towards the smaller side [Fig. 4(b)] because the induced dipole force counteracts the electric field force, reducing the amount of kinetic energy acquired by the electron from the laser field [35]. Similar to the above discussion, when considering the dipole potential in the calculation, the rate of the returning electron distribution will be significantly larger due to the smaller υ_x, giving rise to the considerably higher NSDI ratio.

To offer an intuitive insight into the dipole potential effect, we display two recollision trajectories with time evolution of the induced dipole forces along the x direction (the transverse dimension) in Figs. 5(a) and 5(b). By excluding the dipole potential but with the same initial conditions, it is clearly seen that the electron will be pulled away by the laser field and miss the core, in contrast to the electron trajectory including the dipole potential. This can be attributed to the induced dipole forces attracting the electron along the transverse direction, as indicated by the arrows in Fig. 5. Therefore, considering the attraction of the dynamic dipole potential, the electron will revisit the core more easily, implying that the required υ_x becomes smaller, as shown in Fig. 4(a).

Furthermore, the enhancement of the recollision probability by the dipole potential can be highlighted via the distributions of the distance between the returning electron and the core, and the ratios of the returning electron weight with and without the dipole potential considered, shown in Fig. 6. It is obvious that there are more returning electrons when the dipole potential is considered [Figs. 6(a) and 6(b)]. The ratio in Fig. 6(c) always remains higher than 1 since the returning electrons focused by the dipole potential require smaller υ_x to revisit the core, which is consistent with Fig. 4(a). In addition, this ratio increases as the intensity increases because of the strong dependence of the polarization effect on the intensity [Eq. (5)].

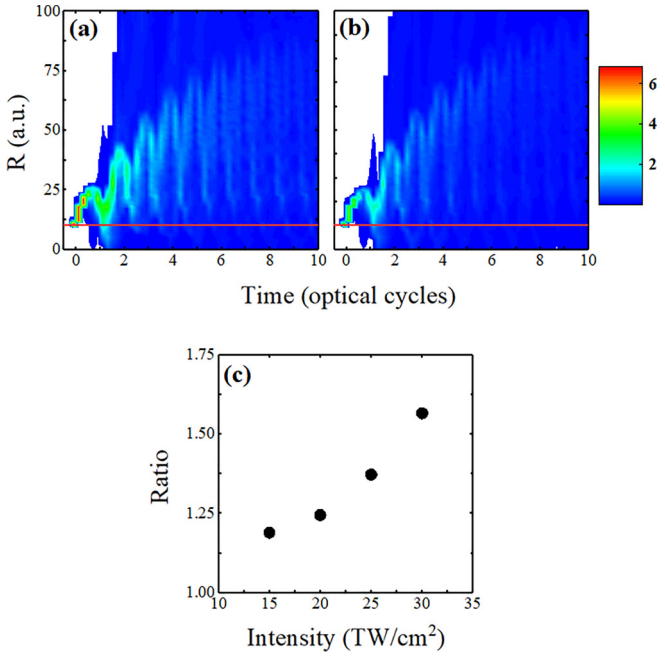

FIG. 6. The distributions of the distance between the returning electron and the core in the first 10 laser cycles at 3×10^{13} W/cm^2, (a) with and (b) without inclusion of the dipole potential. The color scales are the same here. The red lines mark the demarcation of whether the recollision occurs. (c) The ratio between the returning electron weight with and without the dipole potential included vs intensity. The calculation is made with an ensemble of 40 000 trajectories for each panel at 800 nm.

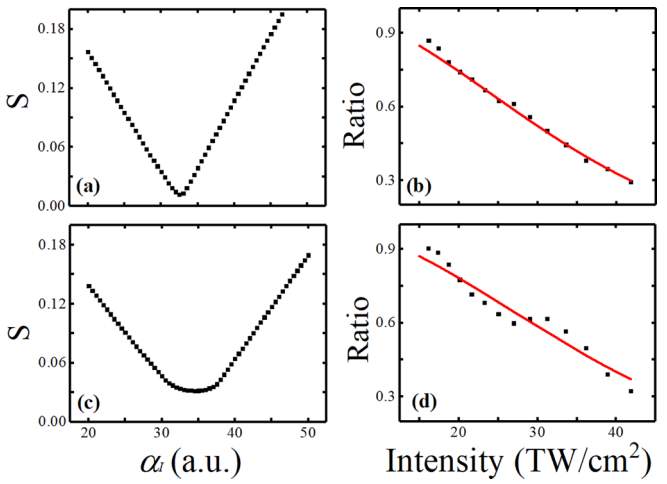

FIG. 7. [(a),(c)] The values of S corresponding to different α_I for 800 and 700 nm, respectively. [(b),(d)] The comparison between $R_i = B_i/A_i$ (black point) and the numerical simulation of Eq. (6) (red line) with $\alpha_I = 32.64$ a.u. and $\alpha_I = 34.49$ a.u. for 800 nm and 700 nm, respectively.

From the above discussion, it is clear that the polarization effects play a prominent role in the recollision-induced double ionization of Mg in CP fields. In turn, we propose a method allowing one to extract the static polarizability of the Mg^+ ion from the ratios of Mg^{2+}/Mg^+. The procedure is described in detail as follows. First, to isolate the polarization effects, we present a "ratio of the ratio," as given by $R_i = B_i/A_i$, where A_i is the ith point of the calculated ratios of Mg^{2+}/Mg^+ with the dipole potential included in the intensity range where NSDI dominates, and B_i is the corresponding calculated ratios obtained from the Monte Carlo simulation ignoring the dipole potential and the Stark shift of the ground state. Both terms are the ones involving α_I in our model. Therefore, the static polarizability of the Mg^+ ion is closely related to R_i. Neglecting the dipole potential and the Stark shift of the ground state, the ratio of Mg^{2+}/Mg^+ can be approximately expressed as $\frac{(2I_p(0))^{1/4}}{5\sqrt{\pi}}\frac{\sqrt{F_0}}{\omega}\exp[-\sqrt{2I_p(0)}\upsilon_c^2/F_0]$ [12], where υ_c is the critical velocity. As the initial transverse momentum υ_x is above υ_c, the tunneled electron can overcome the potential hump and effectively trigger NSDI. In the quasistatic limit, we consider $\omega \to 0$ and obtain $\upsilon_c \approx F_0/\omega$ [12]. As shown in Fig. 4, the dipole potential makes the required υ_x smaller for the returning electrons; correspondingly, υ_c is also smaller. Therefore, when considering the dipole effects, the ratio of Mg^{2+}/Mg^+ is given by $\frac{(2I_p)^{1/4}}{5\sqrt{\pi}}\frac{\sqrt{F_0}}{\omega}\exp[-\sqrt{2I_p}(\upsilon_c - \upsilon_f)^2/F_0]$ with $I_p = I_p(0) + 1/2(\alpha_N - \alpha_I)F_0^2$. The offset momentum resulting from the induced dipole force is $\upsilon_f \approx \frac{2\alpha_I F_0}{\omega|Z_0|^3}$ (see the Appendix), where $Z_0 = I_p/F_0$. We then calculate the result of the following equation:

$$f(\alpha_I) = \left(\frac{I_p}{I_p(0)}\right)^{1/4} \exp\left[\frac{\sqrt{2I_p}(\upsilon_c - \upsilon_f)^2 - \sqrt{2I_p(0)}\upsilon_c^2}{F_0}\right]. \tag{6}$$

Using this equation and the known α_N, we can extract the value of α_I from the simulation of the NSDI ratio. To this end, we get a series of α_I to reproduce R_i by Eq. (6). To estimate the accuracy of α_I, we introduce a formula $S = \frac{1}{N}\sum_i |[R_i - f(\alpha_I)_i]/[R_i + f(\alpha_I)_i]|$, with N the total number of the points used. For each α_I, the corresponding S has different values. For the minimum value of S, we determine the optimized value of α_I.

In the calculations, α_I are uniformly distributed in the interval (20, 50 a.u.) with the adjacent separation $\Delta = 0.01$ a.u. We present the corresponding S for different α_I in Figs. 7(a) and 7(c). It is obvious that S achieves its minimum for $\alpha_I = 32.64$ a.u. (800 nm) or $\alpha_I = 34.49$ a.u. (700 nm), which is very close to the theoretical value of 35.00 a.u. In Figs. 7(b) and 7(d), we exhibit the comparison between $R_i = B_i/A_i$ and the result of Eq. (6) with $\alpha_I = 32.64$ a.u. and $\alpha_I = 34.49$ a.u. for 800 nm and 700 nm, respectively, which satisfactorily reproduce the features of R_i in the chosen intensity range. Because of the applicable range of the Monte Carlo model, the highest intensity in the calculation is limited to $\sim 4 \times 10^{13}$ W/cm^2. Since the NSDI ratio can be measured with a high precision, the method present here can be applied to extract α_I accurately by comparing the experiments with the calculations without dipole potential in the future.

Based on Eq. (5), the polarization effects can be selectively enhanced or weakened by adjusting the laser intensity [16]. Here, we present another effective approach to manipulate the induced dipole force by introducing a three-cycle laser pulse with the carrier-envelope phase (CEP) varied. The pulse

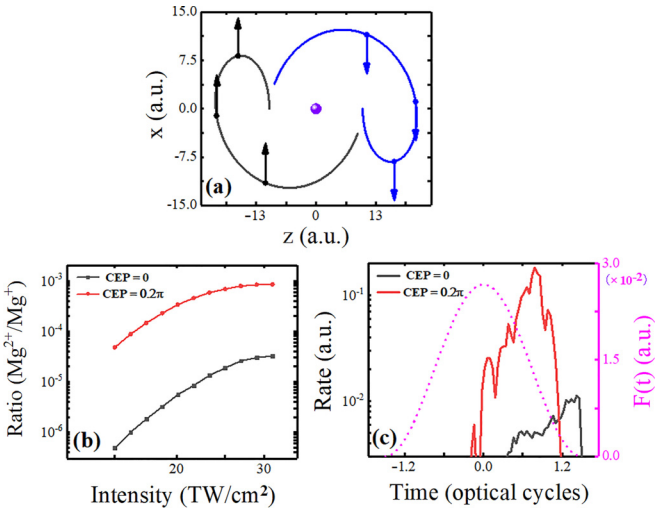

FIG. 8. (a) Two typical electron trajectories in the laser polarization plane at 3×10^{13} W/cm^2 for CEP $= 0$ (black line) and π (blue line), respectively. Both electrons are ionized along the z axis at the peak laser field with the same absolute value of the initial transverse velocity. The purple globe represents the core, and the black dots or blue dots mark the instants around 0.25, 0.5, and 0.75 T after tunneling for each trajectory. The arrows represent the direction of the induced dipole force along the x axis. (b) The calculated ratios of Mg^{2+}/Mg^{+} as functions of laser intensity. (c) The returning time distributions of the first electron and temporal evolution of the electric field envelope (dotted line) at 2.5×10^{13} W/cm^2. The 800 nm, three-cycle cos^2 laser pulses are used here.

envelope is $\cos^2(t\pi/3T)$, where T is the optical period. In Fig. 8(a), we depict two typical returning trajectories for CEP $= 0$ and π, respectively. In these two cases, the electron will be emitted in the opposite direction since the direction of the electric field is flipped. In the two centrosymmetric trajectories, the induced dipole forces are in opposite directions when the freed electrons propagate in the laser field before returning. Thus, the dipole force can be controlled by tuning the CEP. The CEP also plays a key role in the NSDI ratio for the few-cycle laser case, as shown in Fig. 8(b). In order to reveal the underlying mechanism, in Fig. 8(c) we show the returning time distribution of the first electron at the two CEP values of 0 and 0.2π for 2.5×10^{13} W/cm^2. Obviously, the result for CEP $= 0.2\pi$ is closer to the peak of the electric field envelope. According to Eq. (2), the second electron will be ionized much more easily, giving rise to the higher NSDI ratios in Fig. 8(b).

IV. CONCLUSION

In conclusion, we have investigated the effects of the dipole potential on the double ionization probability of Mg for 700 and 800 nm CP fields. We perform a 3D Monte Carlo simulation considering the laser-induced dipole potential. The current studies clearly identify that the dynamic dipole potential enhances the recollision probability. The underlying physical mechanism can be well understood as the returning electrons are focused by the dipole potential, which gives rise to the much higher NSDI ratio. In addition, we introduce a method to determine the static polarizability of the Mg^+ ion from the ratios of Mg^{2+}/Mg^+. We also provide a characteristic knob, i.e., changing the CEP of few-cycle pulses, to control the laser-induced dipole force in NSDI.

ACKNOWLEDGMENTS

This work is supported by the National Key Research and Development Program (Grant No. 2019YFA0307702), National Natural Science Foundation of China (Grants No. 11974380 and No. 12174401), and Science and Technology Department of Hubei Province (Grants No. 2019CFA035 and No. 2021CFA078).

APPENDIX

In the following, we present a simple derivation of v_f. We consider that the recolliding electron leaves the core at time t_0 and returns at time t_r in CP fields. The induced dipole force is given by $\mathbf{F_d} = \nabla[\alpha_I \mathbf{F}(t) \cdot \mathbf{r}/r^3]$. For the return electron, the contribution of the induced dipole force to the momentum becomes [15]

$$\mathbf{P_d} = \int_{t_0}^{t_r} dt \left(\frac{\alpha_I \mathbf{F}(t)}{r^3} - \frac{3\alpha_I [\mathbf{F}(t) \cdot \mathbf{r}]\mathbf{r}}{r^5} \right), \tag{A1}$$

where $r(t_0) = r(t_r) = |Z_0|$. For simplicity, we treat the Coulomb and dipole potentials as perturbations and primarily consider the first returning events [see Fig. 6(a)]. Since the induced dipole force decreases very rapidly with increasing r, $\mathbf{P_d}$ is mainly determined by the part of the electron trajectory close to the tunneling exit, i.e., $r \approx |Z_0|$. When the electron returns to the core, the momentum generated by the external field $\mathbf{F}(t)$ is $-F_0/\omega$ in the transverse direction [36]. Therefore, in such direction, the offset momentum from the induced dipole force is given by

$$v_f = P_{d\perp} \approx \frac{2\alpha_I F_0}{\omega |Z_0|^3}. \tag{A2}$$

[1] R. Dörner, Th. Weber, M. Weckenbrock, A. Staudte, M. Hattass, H. Schmidt-Böcking, R. Moshammer, and J. Ullrich, Adv. At. Mol. Opt. Phys. **48**, 1 (2002).
[2] W. Becker, X. J. Liu, P. J. Ho, and J. H. Eberly, Rev. Mod. Phys. **84**, 1011 (2012).
[3] A. l'Huillier, L. A. Lompre, G. Mainfray, and C. Manus, Phys. Rev. A **27**, 2503 (1983).
[4] P. B. Corkum, Phys. Rev. Lett. **71**, 1994 (1993).
[5] A. D. Shiner, B. E. Schmidt, C. Trallero-Herrero, H. J. Wörner, S. Patchkovskii, P. B. Corkum, J. C. Kieffer, F. Légaré, and D. M. Villeneuve, Nat. Phys. **7**, 464 (2011).
[6] G. G. Paulus, W. Nicklich, H. Xu, P. Lambropoulos, and H. Walther, Phys. Rev. Lett. **72**, 2851 (1994).
[7] D. N. Fittinghoff, P. R. Bolton, B. Chang, and K. C. Kulander, Phys. Rev. A **49**, 2174 (1994).

[8] C. Guo, M. Li, J. P. Nibarger, and G. N. Gibson, Phys. Rev. A **58**, R4271(R) (1998).
[9] G. D. Gillen, M. A. Walker, and L. D. Van Woerkom, Phys. Rev. A **64**, 043413 (2001).
[10] F. Mauger, C. Chandre, and T. Uzer, Phys. Rev. Lett. **105**, 083002 (2010).
[11] X. Wang and J. H. Eberly, Phys. Rev. Lett. **105**, 083001 (2010).
[12] L. B. Fu, G. G. Xin, D. F. Ye, and J. Liu, Phys. Rev. Lett. **108**, 103601 (2012).
[13] J. Dubois, C. Chandre, and T. Uzer, Phys. Rev. Lett. **124**, 253203 (2020).
[14] H. P. Kang, S. Chen, Y. L. Wang, W. Chu, J. P. Yao, J. Chen, X. J. Liu, Y. Cheng, and Z. Z. Xu, Phys. Rev. A **100**, 033403 (2019).
[15] N. I. Shvetsov-Shilovski, D. Dimitrovski, and L. B. Madsen, Phys. Rev. A **85**, 023428 (2012).
[16] H. P. Kang, S. P. Xu, Y. L. Wang, S. G. Yu, X. Y. Zhao, X. L. Hao, X. Y. Lai, T. Pfeifer, X. J. Liu, J. Chen, Y. Cheng, and Z. Z. Xu, J. Phys. B **51**, 105601 (2018).
[17] X. M. Tong, Z. X. Zhao, and C. D. Lin, Phys. Rev. A **68**, 043412 (2003).
[18] X. L. Hao, J. Chen, W. D. Li, B. Wang, X. Wang, and W. Becker, Phys. Rev. Lett. **112**, 073002 (2014).
[19] V. R. Bhardwaj, S. A. Aseyev, M. Mehendale, G. L. Yudin, D. M. Villeneuve, D. M. Rayner, M. Yu. Ivanov, and P. B. Corkum, Phys. Rev. Lett. **86**, 3522 (2001).
[20] G. L. Yudin and M. Y. Ivanov, Phys. Rev. A **63**, 033404 (2001).
[21] A. D. DiChiara, E. Sistrunk, C. I. Blaga, U. B. Szafruga, P. Agostini, and L. F. DiMauro, Phys. Rev. Lett. **108**, 033002 (2012).
[22] G. Gingras, A. Tripathi, and B. Witzel, Phys. Rev. Lett. **103**, 173001 (2009).
[23] I. P. Zapesochnyi, V. A. Kel'man, A. I. Imre, A. I. Dashchenko, and F. F. Danch, Zh. Eksp. Teor. Fiz. **69**, 1948 (1975) [Sov. Phys. JETP **42**, 989 (1975)].
[24] C. Becker, H. Knopp, J. Jacobi, H. Teng, S. Schippers, and A. Muller, J. Phys. B **37**, 1503 (2004).
[25] Z. Zhao and T. Brabec, J. Mod. Opt. **54**, 981 (2007).
[26] N. B. Delone and V. P. Krainov, J. Opt. Soc. Am. B **8**, 1207 (1991).
[27] X. L. Hao, G. Q. Wang, X. Y. Jia, W. D. Li, J. Liu, and J. Chen, Phys. Rev. A **80**, 023408 (2009).
[28] M. Y. Wu, Y. L. Wang, X. J. Liu, W. D. Li, X. L. Hao, and J. Chen, Phys. Rev. A **87**, 013431 (2013).
[29] S. P. Goreslavski, G. G. Paulus, S. V. Popruzhenko, and N. I. Shvetsov-Shilovski, Phys. Rev. Lett. **93**, 233002 (2004).
[30] N. I. Shvetsov-Shilovski, S. P. Goreslavski, S. V. Popruzhenko, and W. Becker, Laser Phys. **19**, 1550 (2009).
[31] M. V. Ammosov, N. B. Delone, and V. P. Krainov, Zh. Eksp. Teor. Fiz. **91**, 2008 (1986) [Sov. Phys. JETP **64**, 1191 (1986)].
[32] A. M. Perelomov, V. S. Popov, and M. V. Terentev, J. Expt. Theor. Phys. (USSR) **50**, 1393 (1966) [Sov. Phys. JETP **23**, 924 (1966)].
[33] C. F. de Morisson Faria and A. Maxwell, Rep. Prog. Phys. **83**, 034401 (2020).
[34] H. P. Kang, S. Chen, Z. Y. Lin, W. Chu, J. P. Yao, W. Quan, J. Chen, X. J. Liu, Y. Cheng, and Z. Z. Xu, Phys. Rev. A **101**, 053433 (2020).
[35] Y. L. Wang, S. G. Yu, X. Y. Lai, X. J. Liu, and J. Chen, Phys. Rev. A **95**, 063406 (2017).
[36] P. B. Corkum, N. H. Burnett, and F. Brunel, Phys. Rev. Lett. **62**, 1259 (1989).